Article:
Jones, SA orcid.org/0000-0002-8579-6444, Bailey, J, Walker, DRE et al. (2 more authors) (2018) Method for Tuneable Homeotropic Anchoring at Microstructures in Liquid Crystal Devices. Langmuir, 34 (37). pp. 10865-10873. ISSN 0743-7463

https://doi.org/10.1021/acs.langmuir.8b01951

Method for tuneable homeotropic anchoring at micro-structures in liquid crystal devices

Sophie A. Jones[1], James Bailey[1,2], David R. E. Walker[3], Guy P. Bryan-Brown[3], and J. Cliff Jones[1]*

[1]School of Physics and Astronomy, University of Leeds, LS2 9JT, UK

[2]Dynamic Vision Systems, Leeds Innovation Centre, 103 Clarendon Road, Leeds, LS2 9DF, UK

[3]DisplayData Limited, Malvern Hills Science Park, Malvern, Worcs. WR13 5SZ, UK

KEYWORDS Surfactant, surface treatment, nematic liquid crystal, homeotropic alignment, anchoring energy, grating alignment, photo-polymer, bistable nematic LCD.

Abstract

A simple method for vapour-phase deposition of a silane surfactant is presented, which produces tuneable homeotropic anchoring in liquid crystals. Both the zenithal anchoring energy and surface slip are measured by fitting to the latching threshold versus pulse width characteristic of a zenithal bistable nematic liquid crystal device based on a deep, sub-micron grating. The method is shown to give microscopic anchoring strength between 5×10^{-5} and 2×10^{-4} J/m^2, with a surface slip of about 100 nm. The silanated surfaces are characterized using Atomic Force

Microscopy (AFM) and X-ray Photoelectron Spectroscopy (XPS), which show a direct relationship between the surface coverage of silane groups and the resulting anchoring energy.

Introduction

Liquid crystals are sensitive to their interaction with contacting surfaces. When used in devices such as displays, surface layers are deposited to give controllable alignment to the liquid crystal director, **n**, the unit-vector that denotes the mean orientation of the long molecular axes. In addition to achieving the appropriate alignment, device performance depends upon the anchoring properties of the alignment layers. A conventional liquid crystal device relies on strong anchoring at the bounding surfaces, such that the anchoring energy is many times higher than typical elastic distortion energies of the **n**-field, thereby ensuring the director at the surface layers remain fixed. However, some devices use low or intermediate anchoring strengths to allow switching of the director at the surface, often to stabilize multiple alignment configurations. Surface switching of the director is required in ferroelectric liquid crystals [1, 2] as well as a variety of bistable nematic displays, including the azimuthal bistable nematic [3, 4], π-twisted bistable nematic (or Binem®) [5] and the Zenithal Bistable Display (ZBD®) [6].

Alignment surfaces in liquid crystal devices impart an easy axis to the director that is either parallel or perpendicular to the surface plane. Methods for LC alignment vary: they include the use of rubbed polymer surfaces and micro-gratings for planar alignment or polymers with pendant aliphatic groups or surfactants for homeotropic alignment [7-9] parallel to the surface normal. The use of surfactants to obtain homeotropic alignment on glass surfaces is long established. For example, reference [10] uses dip-coating from a Langmuir-Bloggett trough to

coat glass plates with controllable density of surfactant, noting a range over which homeotropic alignment was achieved. Liquid phase deposition has been used to produce self-assembled monolayers of thiol [11] and silanes [12 - 15] surfactants with a mixture of chain lengths to control wettability of the surface. Although the results are predominantly on glass surfaces [12 – 14], the method has been applied to micro pillars to illustrate the efficacy for microfluidics [14]. However, as shown in reference [15] the contact angle (and hence surface energy) and surface density of the silane is strongly dependent on the underlying layer: an organic layer formed from a negative photoresist gives a significantly higher surface energy than ITO, which in turn is higher than clean glass. As with previous work, that study varied the surface density by time of exposure to the silane solution and determined the relationship to alignment through the resulting texture of the contacting liquid crystal.

The anchoring strength of the alignment describes the energy cost associated with deforming the LC director away from this easy axis and is frequently written in the Rapini-Papoular form:

$$F_{surf} = W_\theta \sin^2 \theta \quad , \quad (1)$$

where F_{surf} is the surface free energy, W_θ is the zenithal anchoring strength (or equivalently W_φ for azimuthal anchoring strength that is also relevant for planar samples) and θ is a small angle distortion of the director away from the easy axis [16]. Previous measurements of planar anchoring strengths are plentiful, although measurement of homeotropic anchoring considerably less so. In either case, typical values span between 10^{-4} and 10^{-6} J/m^2[17]. A common method is to examine the effects of external torques on the director profile, such as finding the extrapolation length under strong applied electrical or magnetic fields both optically and through cell

capacitance [18-20]. For a homeotropic surface, achieving sufficient accuracy from the electrical determination relies on a nematic with very strong negative dielectric anisotropy, materials that are sometimes difficult to achieve good quality homeotropic alignment. In the absence of external fields, the anchoring strength can be measured through optical characterisation of the director profile or through dynamic light scattering [21, 22]. Such methods often utilise specific cell geometries, such as a wedge cell [23]. These non-perturbative optical methods are restricted typically to the measurement of anchoring strengths below the order of 10^{-4} J/m^2

In ZBD, surface bistability is achieved using a homeotropically-aligned relief grating with a near sinusoidal structure (figure 1). The grating profile is chosen so that the director is forced into either of two elastically deformed states by the homeotropic alignment (rather than lie parallel to the grooves, as it would for a planar aligned surface). The continuous C state has a high-tilt, near vertical alignment, due to the elastic distortion induced by the grating decaying into the bulk of the nematic. In the low-tilt near-planar alignment of the defect D state, the elastic deformation is reduced through the presence disclinations at the top and bottom of the grooves. Latching (that is, switching such that a selected state is retained after application of an electrical field pulse) occurs due to the voltage induced nucleation or annihilation of defects on the side of the grating [6, 24]. There is a significant elastic distortion of the director field in either state close to the surface. This leads to areas of local electric polarity due to the flexoelectric effect [25].

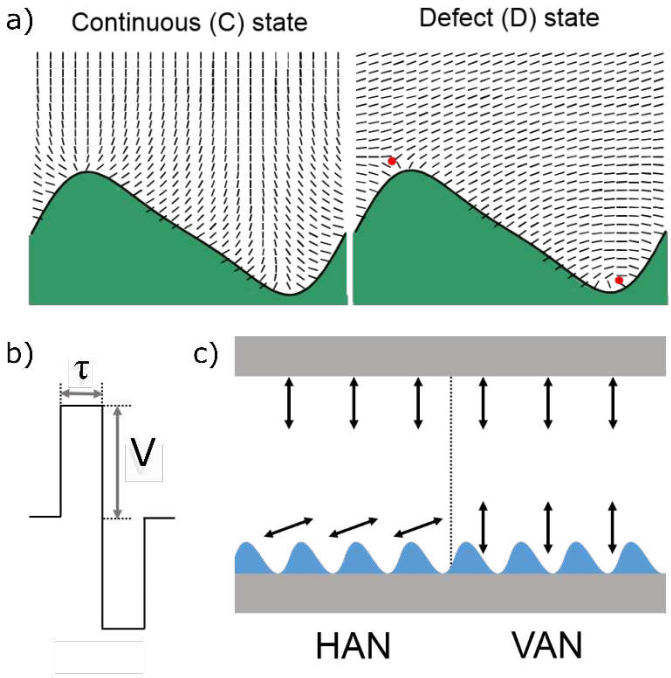

Figure 1. (a) A schematic of the director profile above the ZBD grating for the high-tilt continuous state (left) and the low tilt defect state (right); (b) schematic of the addressing pulse used to latch ZBD from the D to C states, where the trailing pulse is defined as negative for the grating surface. The opposite polarity of pulse (-V,+V) tends to induce latching from C to D ; (c) the two bistable cell configurations given with a grating opposite a homeotropic surface – hybrid aligned nematic (HAN) and vertically aligned nematic (VAN).

A simple 1D model for a flexoelectrically-driven transition between C and D states predicts the latching threshold of a bistable display varies with voltage as [26, 27]:

$$\tau = \frac{\gamma_1 l_s d}{(e_1 + e_3)(V - V_i)} = \frac{A}{V - B} \qquad (2)$$

where γ_1 is the rotational viscosity of the nematic, l_s is the surface viscosity or slip length, d is the cell gap, $(e_1 + e_3)$ is the sum of the splay and bend flexoelectric coefficients of the nematic, and τ and V are the electric impulse duration and amplitude. A and B are the two critical parameters used to calculate the slip and anchoring strength during fitting. The divergent threshold V_i is related to the anchoring strength by:

$$V_i = \frac{2W_\theta d}{(e_1 + e_3) + \sqrt{\epsilon_o \Delta\epsilon K_{33}}} \qquad (3)$$

where ϵ_o is the permittivity of free space, $\Delta\epsilon$ is the dielectric anisotropy of the LC, and K_{33} is its bend elastic constant [27]. Further to the work of reference [27], these equations use the assumptions that there is minimal offset of the grating from the electrode surface and that the grating dimensions are sufficiently lower than the cell gap. That is, the dielectric terms associated with grating shape contributes about an extra 0.5 micron cell gap, which is similar to the difference in cell gap measured when measured outside the grating area. Hence, the factor of grating shape can be ignored in this calculation. Collecting the pulse thresholds under a range of different parameters allows the data to be fit for both the zenithal anchoring strength W_θ and slip length l_s. For the one-dimensional theoretical model used, variations of the grating shape can only be included through the dielectric terms as mentioned above or through the anchoring term W_θ itself. However, comparison between the one-dimensional model that yields the analytical equation in reference [26] and the two-dimensional Q-tensor modelling of reference [27] showed

excellent agreement. Hence, it is postulated that the treatment used here gives a satisfactory approximation to the absolute value of the local surface anchoring energy. The method certainly provides means for determining the relative values of the zenithal anchoring energy.

Equations (2) and (3) indicate a strong dependence of the operating voltage of the display on the zenithal anchoring energy of the surface, particularly when low voltages are used. Commercial ZBD devices use a proprietary homeotropic photopolymer layer to form the appropriate grating [28], thereby ensuring that variability of the anchoring energy is minimised. Using conventional liquid phase deposition methods [e.g. 13, 15] to coat the ZBD grating surface leads to a wide partial latch region of the threshold characteristic, due to variations of the anchoring energy. The lack of reproducibility and heterogeneity of liquid phase deposited silanated films was also noted in [12], and these problems are potentially exacerbated by depositing onto a polymer surface instead of glass. Previously, [29] surface assembled monolayers of surfactants deposited through liquid phase and vapour phase deposition techniques have been compared and the latter method shown to give better reproducibility. This finding is supported in this work too, where devices made using vapour phase deposition of a silane give reproducible and uniform latching of a ZBD device that is comparable to the homeotropic photopolymer. Moreover, the strong dependence of the latching pulse impulse on the anchoring energy offers a means by which the zenithal anchoring energy may be measured.

In the current work, a photopolymer is designed using off-the-shelf components instead and vapour-phase deposition of a silane surfactant is used for obtaining and measuring a tuneable anchoring strength. A simple, practical method is proposed to coat a substrate with the surfactant uniformly and is used to achieve a range of different anchoring energies through control of the silane surface density, characterized as a benchmark for comparable systems by Atomic Force

Microscopy (AFM) and X-ray Photoelectron Spectroscopy (XPS). The method does not require specialist equipment and is readily set up in a conventional laboratory. Moreover, it is shown to give controllable and reliable homeotropic anchoring even on non-uniform surfaces. By presenting the photopolymer composition alongside the surface treatment method, the results are readily-applicable to other systems involving nano- and micro- structures within liquid crystal devices. Together with the measured anchoring energy and slip lengths, the approach promises great applicability for novel applications of liquid crystals where alignment control is required on a photopolymer, including devices with structured surfaces and walls (such as microfluidic systems), and with colloidal and particulate inclusions.

Experimental

The conventional method for imparting micro-relief structures onto surfaces is nano-imprint lithography (NIL) [30]. However, where microstructures are to be used in conjunction with electric fields orthogonal to the surface, it is important to minimise the offset between the bottom of the microstructure and the surface electrode. Not only does such offset cause an unwanted voltage drop and waste power, minute variations of the offset thickness cause large variations in the applied electric field across the contacting liquid crystal, particularly in devices where the difference in electric permittivity of the photopolymer and liquid crystal is high. It is impractical to use conventional NIL and other stamping methods to obtain minimal offset over anything but the smallest area, since the structure impedes fluid flow during the stamping process except where there is offset. Instead, an embossing method is preferable [31] where the inverse microstructure is formed onto a flexible backing film, placed onto the substrate with a

reservoir of uncured photopolymer at one edge, and embossed from that side of the substrate to the other using a rubber-coated roller. With this technique, the tops of the inverse-microstructure are pushed into contact with the substrate and the excess fluid can flow away from the roller contact line due to the film flexibility. As the roller moves across the film and substrate, the liquid photopolymer is pushed ahead of the line of contact between the microstructure and substrate, whilst filling the gaps created by the microstructure features. Once the roller has passed across the substrate, capillary forces hold the film in place, allowing the photopolymer to be cured separately. Indeed, this method has the advantage that precise micro- and nano-scopic structures can be deposited in an acrylate photopolymer and cured in the presence of oxygen and without need of a nitrogen atmosphere that inhibits the cure. The film used for the current study was pre-fabricated by DisplayData by roll-to-roll embossing of a resin-coated PET film using a nickel shim copied from the original photo-resist master grating with the required structure using electro-forming.

The liquid crystal test devices used in the current work comprised one substrate with a grating embossed into the photopolymer PP2, figure 2. A 5cm diameter steel roller with a 5mm thick rubber coating of shore hardness 70 was embossed with an 800N downward force on the film, photopolymer and substrate, (corresponding to about 0.2N/mm^2) and a lateral linear speed of about 0.5mm/s across the substrate, The photopolymer PP2 was a mixture of acrylate monomers Sartomer 508 (57% by weight) and Sartomer 349 (38% by weight) with 5% of the photo-initiator Genocure LTM. The composition of this photopolymer was chosen to give a viscosity of 70 cP, suitable for fast embossing speeds. Sartomer 349 and 508 contain minor components which are hydroxyl-terminated monoesters. These are from incomplete conversion of the diol precursors. Methacrylate analogues are also likely to contain small amounts of these

hydroxyl-bearing intermediates as they are produced via similar (trans)esterification processes. The residual hydroxyl groups may help to ensure a uniform and reliable coating through covalent bonding of the silane. The results of reference [27] were made using another methacrylate photopolymer mixture and similar results were found in that work. However, reproducibility and lifetime are better assured in this mixture.

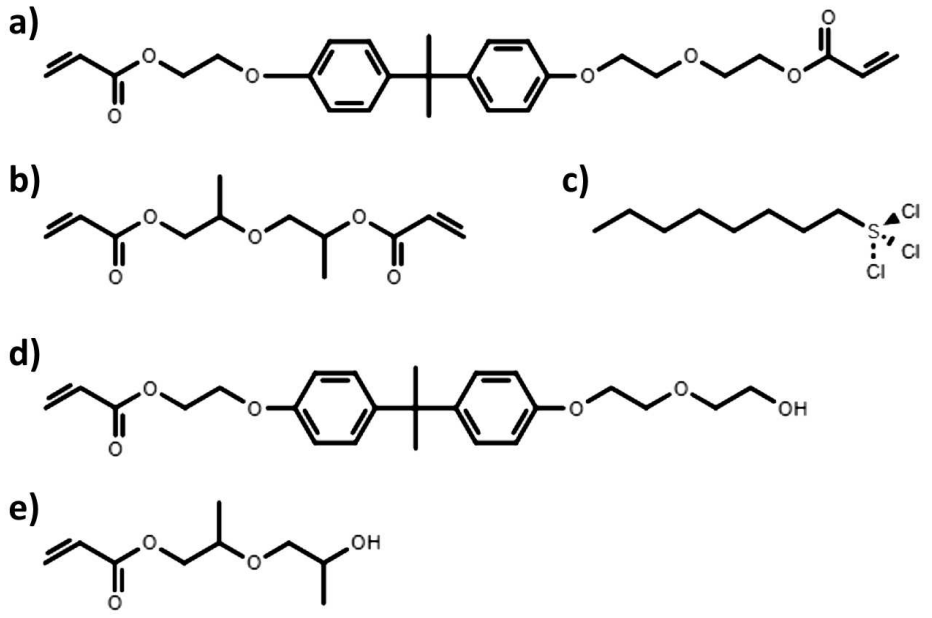

Figure 2. Chemical structures for the PP2 monomers: a) Sartomer 349, b) Sartomer 508, and c) the silane surfactant C8-Sil [Sartomer]. Also presented are the monoester impurities of Sartomer 349 and 508, d) and e) respectively. These impurities were measured at 4.9 and 6.8 %w/w within the components as sold.

For the surface treatment, the photopolymer substrate is cleaned using UV-O3 for five minutes. A purpose-built evaporator unit was built to control the deposition of silane onto the photopolymer gratings, shown in figure 3. The chamber was formed from the lower section of a 25cm diameter glass desiccator with a polypropylene lid. The sample substrate is mounted onto a

horizontal stage rotating at approximately 10 rpm within the chamber, which is sealed. A fixed volume of 20 μL of trichloro octyl (C8) silane is deposited into a flask and heated to 80 °C. Compressed air at 0.8bar is passed through the flask at 0.01 m^3/s, where it mixes with silane vapour and passes into the sample chamber via plastic tubing with a 9mm internal diameter. The tubing is mounted within a copper pipe that is also heated to about 80 °C using an electric blanket to prevent premature condensation of the silane vapour within the tubing. An 80 mm diameter fan is used to circulate the silane within the chamber for uniform deposition over the rotating sample. The vapour leaves the chamber through an HCl capture system. This comprised bubbling the excess vapour through indicator solution before passing it through steel wool, to prevent the HCl vapour produced by the silanation reaction from escaping into the laboratory. The surface density of silane that condenses on the substrate may be controlled using the exposure time. Alternatively, if the humidity and temperature of the lab are variable, then the process can be monitored using a commercial HCl gas sensor. However, continuous assessment showed that the setup was sufficiently controllable and reproducible such that an HCl gas sensor would have been an unnecessary addition, with the humidity of the laboratory in the experiments being controlled to 40% ± 5%. Once the process is completed, the substrates are baked at 180°C for 1 hour on a hot plate to complete the silanation reaction. The silane chamber is thoroughly cleaned with acetone and isopropanol after each sample run, to prevent build-up of surfactant on the chamber walls, and thereby change the proportion of silane surfactant deposited onto the substrate surface.

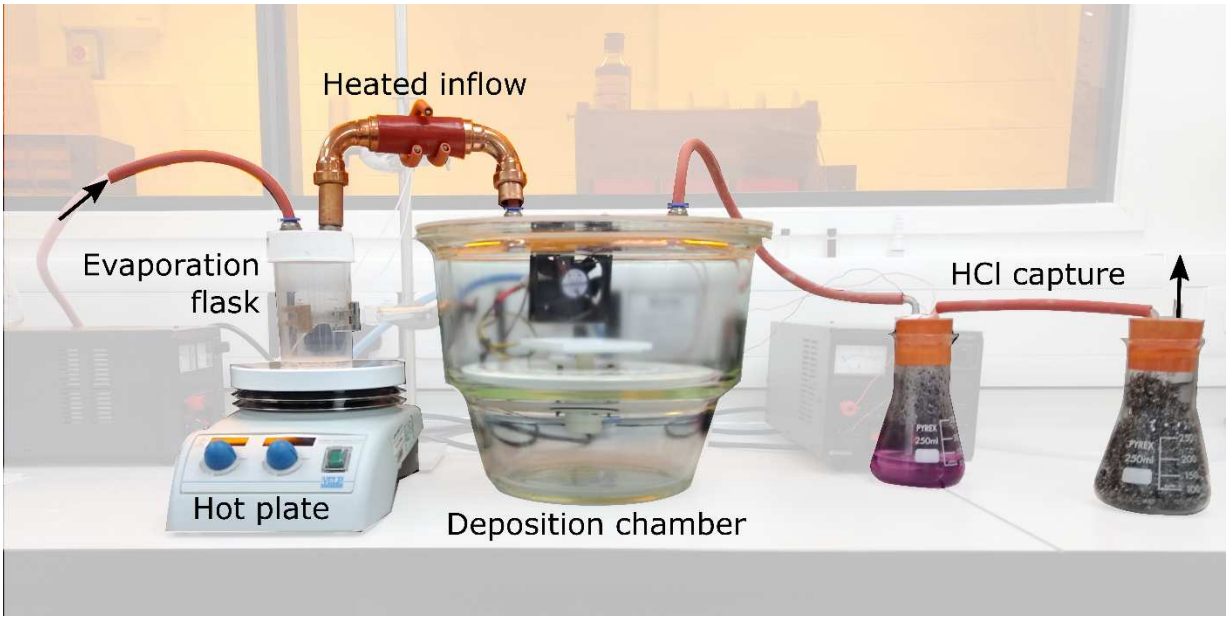

Figure 3. Schematic of the silane deposition rig. Arrows indicate the initial inflow of compressed air and the final outflow, after two HCl capture steps.

The resulting surface density of silane versus exposure time was characterised using XPS. Photopolymer flats were treated in the same instance as the grating test substrates and the XPS data collected in order to determine the progression of the surface treatment throughout the experimental timeframe. XPS measurements were performed using a Thermo Escalab 250 XPS with monochromated aluminium K-alpha X-ray source. The samples were mounted onto carbon tape for analysis. The spot size was 500 μm with a power of 150W. Detailed spectra of individual peaks were taken at energy of 20 eV with a step size of 0.1 eV, the number of scans for each element was optimised to give a good signal to noise for each element. Binding energy was calibrated by setting the carbon 1s spectral peak to 285eV. Detailed spectra had a Shirley or

linear background fitted to them and peaks were fitted and de-convoluted using mixed Gaussian-Lorentzian fits (using CASAXPS).

Test LCD cells were constructed with an ITO-coated glass flat substrate coated with the homeotropic polyimide SE1211 (Nissan) opposite the embossed and silanated PP2 grating surface, spaced using 5 μm glass beads. Each substrate had a 1 cm^2 electrode area fully covered on one side with the embossed photopolymer grating. Cell gaps were measured using reflection spectrometry. Each completed cell was filled with the liquid crystal 4-cyano-4'pentyl biphenyl (5CB), chosen for the wealth of characterisation data available through literature. The use of an opposing homeotropic surface gives the cell hybrid-aligned nematic (HAN) and vertically-aligned nematic (VAN) as the bistable configurations for the D and C states, respectively, figure 1. The two states are readily discriminated using polarising optical microscopy, with the grating aligned 45° to the crossed polarisers to give a bright D state and dark C state. Each cell was capillary filled at room temperature in the direction parallel to the grating grooves. The area of the grating that spontaneously formed the D and C states was recorded, before heating into the isotropic phase and cooling back into the nematic phase to form the uniform D state.

The critical voltages for a range of impulse durations (τ) were found at which the alignment latched from the continuous into the defect state, C - D. Data were fit to the theoretical model of equation (2) using non-linear least squares regression with two free parameters A and B, from which values for the slip length and anchoring strength were calculated. The following literature values for the flexoelectric coefficients, dielectric anisotropy, twist viscosity and elastic constant were used for 5CB at 25 °C: e_1+e_3 = 14.5 pC/m [32], $\Delta\varepsilon$ = 13.15 [33], γ_1 = .099 Nsm^{-2} [34], and K_{33} = 8.25 pN [33].

Results and Discussion

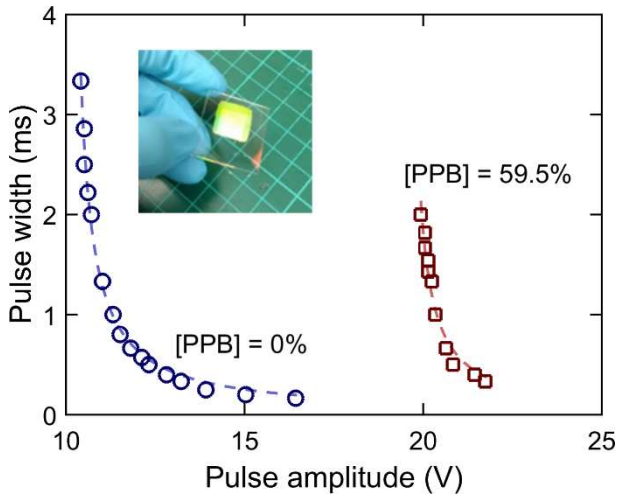

Figure 4. An example of the data points and fitted curves for the field induced C to D transitions of grating aligned LC devices in which the grating is formed using two spontaneously homeotropic photopolymers with different anchoring energies. Inset is an image of a single cell plate, highlighting the embossed grating area. Both cells were nominally 7 μm in cell gap, operating at 25 °C in VAN/HAN mode and filled with the nematic liquid crystal pentyl cyanobiphenyl (5CB).

Before measuring the anchoring of the silanated photopolymer, devices with the proprietary homeotropic-aligning photopolymer mixture previously studied in reference [35] were tested for comparison. Tuning of the anchoring energy is done in the commercial displays by mixing a high anchoring energy photopolymer (PPB) into a low anchoring base photopolymer (PPA) (obtained from Displaydata Ltd.). This is used in the commercial process to compensate display operating voltages against variations in the original master used to produce the embossing film. These photopolymers are designed to span the window of bistability in ZBD.

Figure 4 shows the 5CB 25. ± 0.1°C latching voltages for 7. ± 0.1 μm spaced ZBD for pure PBA and a 40.5 wt.% PPA + 59.5 wt.% mixture of the photopolymers, showing the latching voltage changing between 10 V to 20 V for this grating. Fitting the resultant electro-optic characteristic to equations (2) and (3) for various concentrations shows that the latching voltages vary linearly with concentration of PPB between 3×10^{-5} and 9×10^{-5} J/m^2,figure 5 a).

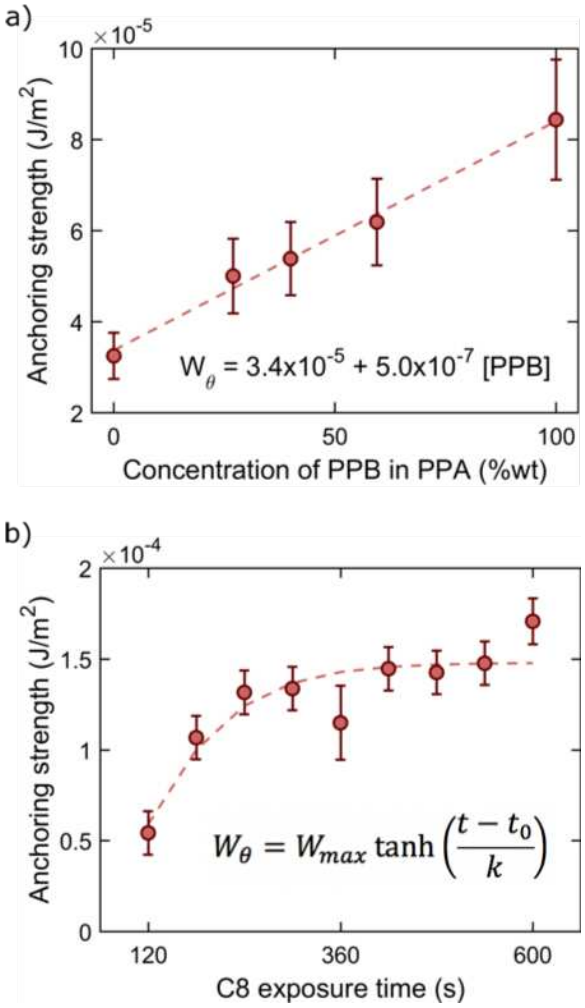

Figure 5. Grating anchoring strength results for a) the mixed photopolymers, and b) the silanated photopolymer. A linear fit is included for the photopolymer mixtures, whereas the silanated cells are fit to equation (4), with W_{max} = (1.5 ± 0.1) x 10^{-4} N/m, t_0 = (57 ± 10) s and k = (151 ± 30) s.

Varying the C8 exposure time for PP2 gratings gave bistable alignment between 120 sec and 600 sec exposure. At lower exposure times, the homeotropic anchoring was too weak to form vertical alignment. In the resulting conical alignment, the director lies at some in-plane angle to the groove direction, rather than perpendicular to the grooves (and parallel to the grating vector) as in the correct bistable state. Above 600 sec the alignment began to appear patchy and inconsistent, and the operating voltages began to approach the dielectric breakdown of the grating surface. Photomicrographs of the textures for the range of exposure times are shown in figure 6, both for that formed directly on filling and for the operating state formed after cooling from the isotropic phase. Figure 5 b) shows that the anchoring energy tends to increase with exposure time. An empirical fit to the data suggests the approximate relationship:

$$W_\theta = W_{max} \tanh\left(\frac{t - t_0}{k}\right) \qquad (4)$$

where the anchoring energy W_θ plateaus to W_{max} with increasing treatment time t, t0 is the threshold time required to give homeotropic alignment and k is the fitting constant. In comparison with the mixed photopolymers, silanation of PP2 gives much higher anchoring, ranging from intermediate to strong. This is not an ideal range for the bistable device as it correlates to increasing latching voltages. For instance, the 600 s exposure time represents an operating voltage of around 45 V for 5CB. However, stronger anchoring has applications elsewhere and is more generally of interest in conventional display devices.

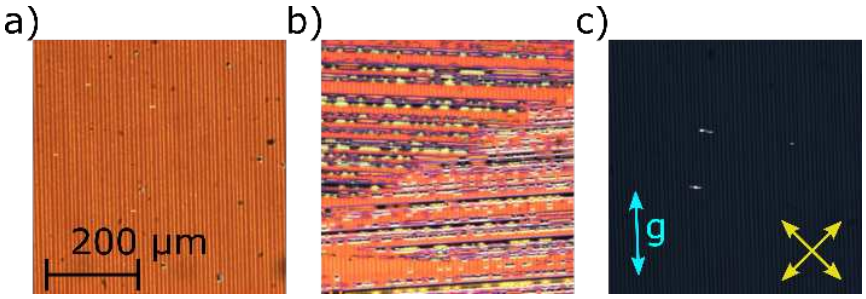

Figure 6. First filling states for a) 180, b) 300, and c) 600 s exposure times, showing adoption of D state, mixed, and C state, respectively, correlating with increasing anchoring strength. Each cell cooled from isotropic into uniform D state. The position of crossed polarisers is indicated, as is the direction of the grating vector, g.

Conventional silane surface treatment is done in vacuum, where quantities of silane and water are introduced instantaneously into the chamber containing a silicon or glass substrate that has been pre-treated with O_2 plasma, to ensure that the surface is covered with OH groups [36]. In those circumstances, the silane deposits onto the surface as a monolayer, reacting with the abundant surface hydroxyl groups, therein giving off HCl vapour. The surface layer is completed when the water causes a condensation reaction to form further Si-O-Si bonds between adjacent surface silane molecules [36]. The current procedure is designed to coat a photopolymer that has scarce hydroxyl groups onto which the silane bonds covalently. Instead, an almost epitaxial approach is taken, where the surfactant is slowly introduced into the chamber to form only rare covalent bonds directly to the photopolymer. Once bonded to the surface, the atmospheric water continues to react with the remaining Si-Cl groups to provide two new surface hydroxyl sites onto which further silane vapour deposits, as shown schematically in figure 7. If the exposure

time is too great and the surface covered, the silane continues to react increasingly forming a polymer above the surface.

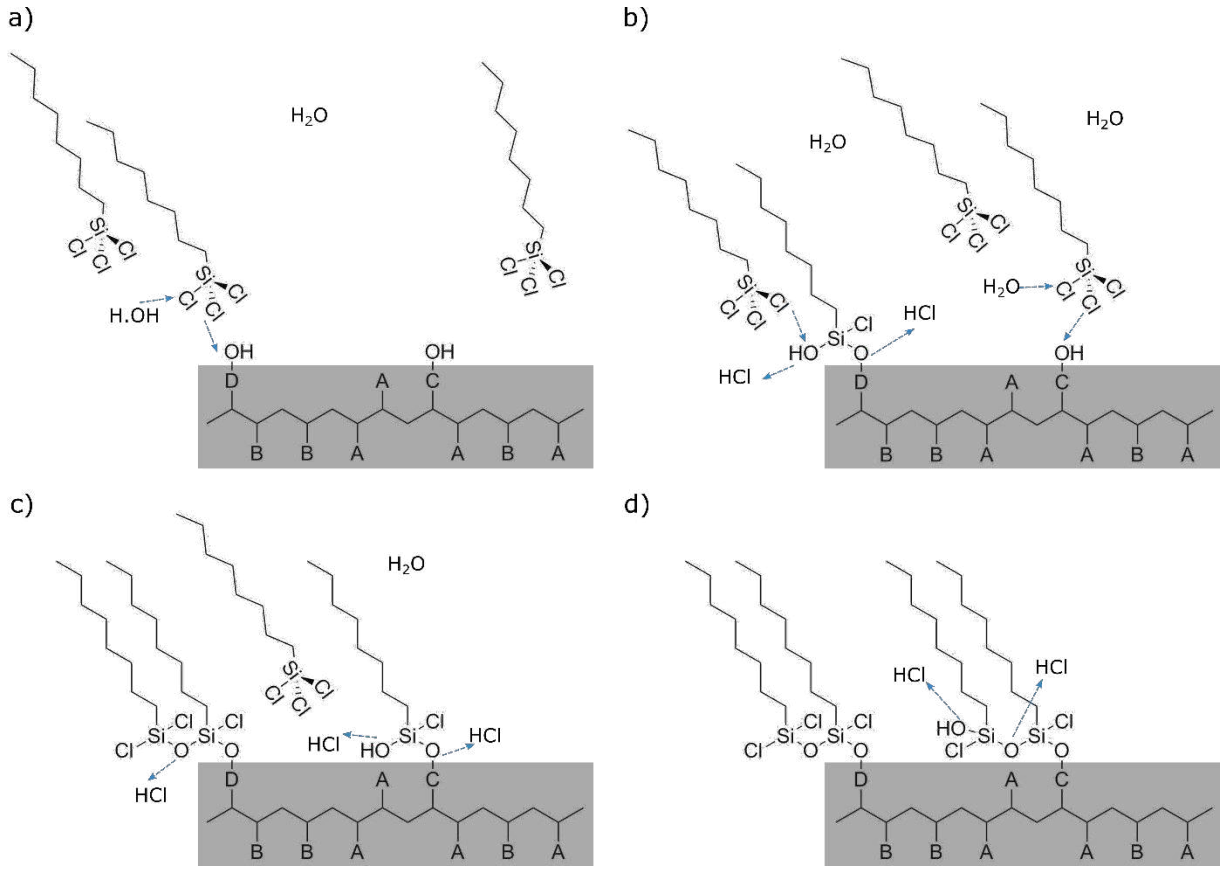

Figure 7. Schematic of the silanation reaction, progressing from monolayer formation to condensation. The photopolymer surface is simplified as shown, where A is Sartomer 349 residual structure, B is Sartomer 508 residual structure, C is the hydroxyl-bearing Sartomer 349 monoester residual structure, D is the hydroxyl-bearing Sartomer 508 monoester residual structure.

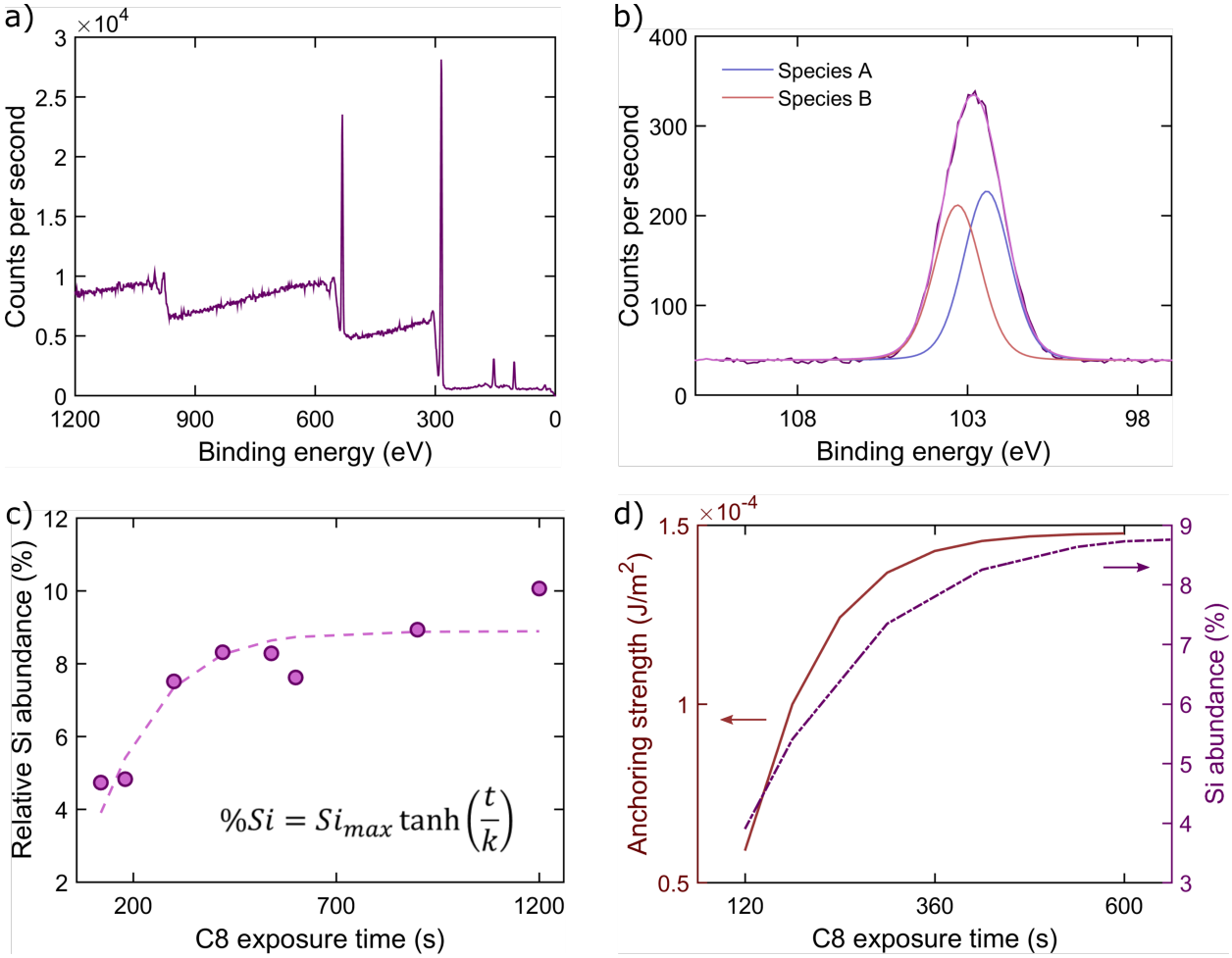

Figure 8. XPS results are presented. (a) shows the full spectrum obtained for the 540 sec exposure sample. Full scans were recorded for the carbon 1s, oxygen 1s, nitrogen 1s, and silicon 2p. No evidence of Cl was found in the surface. (b) shows the breakdown of both fitted species in the same sample. Relative Si abundance is plotted against exposure time in (c) and the fitting shown with the anchoring fit in (d). The XPS data were fit to the same form as equation (4), with Si_{max} = (8.8 ± 0.5) %, t_0 = 0 s and k = (260 ± 20) s.

Amongst the XPS peaks observed from the photopolymer flats, two corresponded to the silicon counts. Detailed spectra were taken of the silicon-2p peaks, and species were assigned using literature values to Si-O-Si bonds (102.5 eV) and SiO_2 bonds (103.3 eV), respectively, figure 8 [37, 38]. No peak was found for Cl, indicating that the silane condensation reaction was complete, and that all Cl had escaped as a gas. No Si was detected for the plane sample without silanation, indicating that the photopolymer covered the glass substrate entirely. The density of Si correlates well with the anchoring strengths, as seen in the plot of figure 8 d).

Clearly, there is a good correlation between silanation time, total Si detected on the surface by XPS and the anchoring energy measured using the bistable grating devices. There are two potential models for the silane coating. In a first "island" model [39], the silane forms sub-micron domains of strongly anchored, highly silanated surface interspersed with areas of uncoated photopolymer such that the size of the domains increases with exposure time. The microscopic length scales of these domains are averaged by the liquid crystal, to give homeotropic anchoring that is directly proportional to the surface density of the pendant silane groups. Alternatively [40], the silane may attach to the surface relatively uniformly over the area of exposure, and the density of the silane increase with exposure time. Figure 9 shows tapping-mode AFM images from samples taken from across the range of exposure times. These results show that there is a decrease in surface roughness with increasing exposure time from 1 nm to below 0.5 nm and with no evidence for silane domains on the 500 nm length scale. If the first model were true, surface roughness would initially increase; hence, the results support the second, uniform growth model. It would be instructive to test whether this was due to the high density of hydroxyl groups present in the photopolymer PP2, or whether this behaviour is universal for any polymer surface.

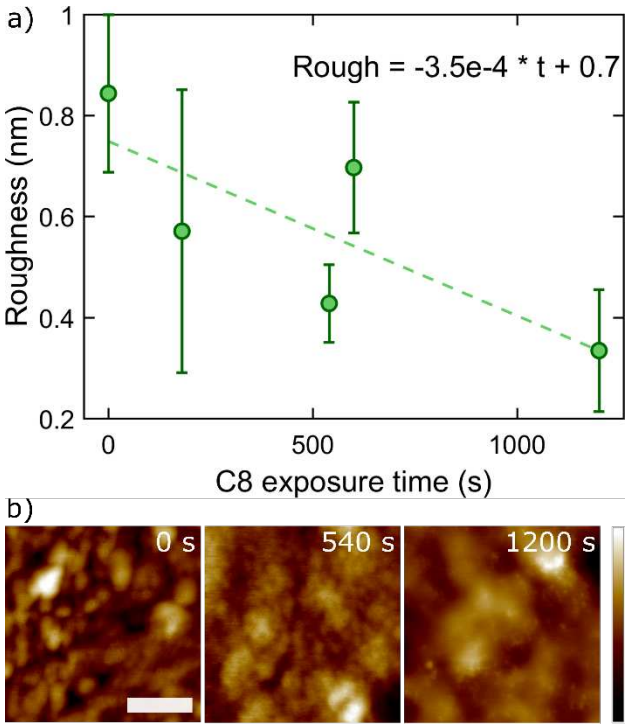

Figure 9. a) Measured surface roughness with silane exposure time and b) AFM micrographs of the polymer surface. Each is a 500 nm x 500 nm area, flattened for analysis. Surface roughness was determined by averaging several 100 nm x 100 nm areas for each sample – a 100 nm scale bar is included. The colormap shown denotes 5 nm (white) to -5 nm (black).

In addition to anchoring strength, fits to the latching characteristic also yield values for the slip length, the surface viscosity term that indicates the extrapolated depth within the surface where liquid crystal flow no longer occurs and the boundary for no-slip can be extrapolated [41]. In general, viscous fluids are expected to have a shorter slip length because they are less likely to exhibit flow at the surface. The authors are unaware of previous measurements of the surface slip length for liquid crystals. The slip length of the mixed photopolymer surface was of the order of tens of nanometres and reduced only slightly with increasing concentration of the high anchoring

photopolymer, although the change was small and comparable to the experimental errors (figure 10 a)). This is sufficiently small to agree with the no-slip treatment of liquid crystals. However, the slip length of the C8-silane treated gratings was found to be of the order of hundreds of nanometres, again decreasing slightly with increasing surface density (figure 10 b)). It is hypothesised that the larger slip length in this case indicates that the silane molecules are sufficiently rarefied at the surface thereby allowing flow of the liquid crystal between the silane pendant chains. That is, the grating surface has a region that contains both silane and liquid crystal, and that this boundary becomes better defined as the silane density increases with increasing exposure time. These values for slip length are relevant to other devices using homeotropic boundary conditions, such as the Vertically Aligned mode for TV and monitor applications.

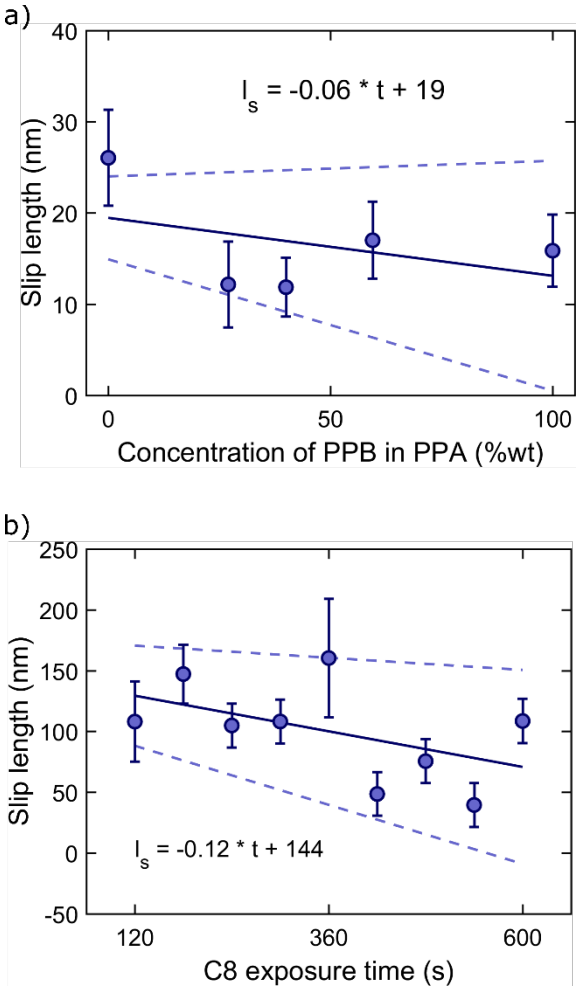

Figure 10. Slip length at the homeotropic grating surface for the mixed photopolymers (a) and the silanated PP2 (b). Linear fits are included as guides, with the upper and lower fits given with respect to the standard errors on the fit.

Conclusions

By varying exposure time to warm C8 silane, anchoring strength at a photopolymer surface was controlled and measured as a function of time, which correlates well with measured silicon via XPS and decreasing roughness of the photopolymer surface via AFM. These measurements are

in agreement to previous values, as is seen when the method is compared to previous results within the same system. Values are as expected for intermediate anchoring.

Each element of this study together, including the photopolymer, silanation apparatus and method, and measurement technique, is proposed as a replicable method for homeotropic anchoring and measurement in novel liquid crystal devices. Such devices often employ nano- or micro-structures formed from photopolymer; this method allows for known and tuneable homeotropic anchoring at such surfaces. The use of XPS gives a grounding by which similar techniques may be mapped to those presented here.

AUTHOR INFORMATION

Corresponding Author

*j.c.jones@leeds.ac.uk

Author Contributions

The manuscript was written through contributions of all authors. All authors have given approval to the final version of the manuscript.

Funding Sources

SJ is grateful to the Displaydata Ltd and the School of Physics and Astronomy at Leeds for funding. JCJ also wishes to thank the EPSRC for an Advanced Fellowship in Manufacturing (EP/L015188/2).

Acknowledgement

The authors wish to thank Drs. Ben Johnson and Peng Bao of the Molecular and Nano Physics Group at the University of Leeds for help with the XPS and AFM, respectively, and Nikita Solodkov for useful discussions. The data for the current work is given in reference [42].

Abbreviations

AFM, Atomic Force Microscopy; HAN, hybrid aligned nematic; LC, liquid crystal; PP, photopolymer; VAN, vertically aligned nematic; XPS, x-ray photoelectron spectroscopy; ZBD, zenithal bistable device.

References

[1] Clark, N. A.; Lagerwall, S. T., Submicrosecond bistable electro-optic switching in liquid crystals. *Appl. Phys. Lett.*, **1980**, *36*, 899.

[2] Xue, J.; Clark, N.A. and Meadows, M.R., Surface orientation transitions in surface stabilized ferroelectric liquid crystal structures. Appl. Phys. Lett., **1988**, 53, 2397

[3] Durand, G.; Barberi, R.; Giocondo, M.; Martinot-Lagarde, P. R. Nematic liquid crystal display with surface bistability and control by flexoelectric effect. *US patent 5357358A*, **1990**.

[4] Bryan-Brown, G. P.; Towler M. J.; Bancroft, M. S.; McDonnell, D. G. Bistable nematic liquid crystal device. *GB patent 2286467A*, **1994**.

[5] Dozov, I. N.; Martinot-Lagarde, P. R.; Polossat, E.; Lelidis, I.; Giocondo, M.; Durand, G. E. Fast bistable nematic display from coupled surface anchoring breaking. *Proc. SPIE 3015, Liquid Crystal Materials, Devices, and Applications V*, **1997**.

[6] Bryan-Brown, G. P.; Brown, C. V.; Jones, J. C.; Wood, E. L.; Sage, I. C.; Brett, P.; Rudin, J. Grating aligned bistable nematic device. *SID Digest volume XXVIII*, **1997**, *5.3*, 37-40.

[7] Geary J. M.; Goodby, J. W.; Kmetz, A. R.; Patel, J. S. The mechanism of polymer alignment of liquid crystal materials. *J. App. Phys.*, **1987**, *62*, 4100.

[8] Flanders, D. C.; Shaver, D. C.; Smith, H. I. Alignment of liquid crystals using submicrometer periodicity gratings. *Appl. Phys. Lett.*, **1978**, *32*, 597.

[9] Creagh, L. T.; Kmetz, A. R. Mechanism of surface alignment in nematic liquid crystals. *Mol. Cryst. Liq. Cryst.,* **1973**, *24*, 59-68.

[10] Hilltrop, K; Stegemeyer, H; On the orientation of liquid crystals by monolayer of amphiphilic molecules. IN Griffin, A.C.; Johnson, J.E.; (Eds.) Liquid Crystals and Ordered Fluids, Volume 4; Plenum Press, **1984,** 515 – 530.

[11] Drawhorn, R.A.; Abbott, N.; Anchoring of Nematic Liquid Crystals on Self-Assembled Monolayers Formed from Alkanethiols on Semitransparent Films of Gold *J. Phys. Chem.,* **1995**, *99,* 16511.

[12] Evans, S.D.; Allinson, H.; Boden, N.; Henderson, J.R.; Surface-field induced organisation at solid/fluid interfaces. *Faraday Discuss.*, **1996**, *104,* 37-48

[13] Liao, Y.-J.; Hsu, C.-S.; Wu, S.-T. Dipping and Photo-Induced Liquid Crystal Alignments Using Silane Surfactants. *Jpn. J. Appl. Phys. Lett.* **2000**, *39,* L90–L 93

[14] Noonan, P. S.; Shavit, A.; Acharya, B.R.; Schwartz, D.K. Mixed alkyl silane functionalized surfaces for simultaneous wetting and homeotropic anchoring of liquid crystals. *ACS Appl. Mater. Interfaces* **2011**, *3,* 4374–4380

[15] Son, J.-H.; Zin, W.-C.; Takezoe, H.; Song, J.-K. Alignment of Liquid Crystals Using a Molecular Layer with Patterned Molecular Density. *Adv. Mater.* **2012**, *24,* 6105–6110

[16] Rapini, A.; Papoular, M. Distorsion d'une lamelle nématique sous champ magnétique conditions d'ancrage aux parois. *J. Phys. (France) Lett.,* **1969**, *C4*, 54.

[17] Jérome, B. Surface effects and anchoring in liquid crystals. *Rep. Prog. Phys.* **1991**, *54*, 391-451.

[18] Fonesca, J. G.; Charue, P.; Galerne, Y. Zenithal anchoring angle and anchoring strength on oxidized silane plates. *Mol. Cyst. and Liq. Cryst.*, **1999**, *329*, 597-604.

[19] Yokoyama, H. Surface anchoring of nematic liquid crystals. *Mol. Cryst. Liq. Cryst.*, **1988**, *165*, 1.

[20] Yokoyama, H.; van Sprang, H. A. A novel method for determining the anchoring energy function at a nematic liquid crystal wall interface from director distortions at high fields. *J. Appl. Phys.*, **1985**, *57*, 10.

[21] Fonesca, J. G.; Galerne, Y. Simple method for measuring the azimuthal anchoring strength of nematic liquid crystals. *Appl. Phys. Lett.*, **2001**, *79*, 2910.

[22] Vilfan, M.; Copic, M. Azimuthal and zenithal anchoring of nematic liquid crystals. *Phys. Rev. E.*, **2003**, *68*, 031704.

[23] Gwag, J. S.; Yi, J.; Kwon, J. H. Determination of actual surface azimuthal anchoring strength using a wedge-shaped liquid crystal cell. *Optics Lett.*, **2010**, *35,* 456-458.

[24] Parry-Jones, L. A.; Elston, S. J. Flexoelectric switching in a zenithally bistable nematic device. *J. Appl. Phys.,* **2005**, *97*, 093515.

[25] Meyer, R. B. Piezoelectric effects in liquid crystals. *Phys. Rev. Lett.*, **1969**, 22, 918

[26] Davidson, A. J.; Mottram, N. J. Flexoelectric switching in a bistable nematic device. *Phys. Rev. E*, **2002**, *65*, 051710.

[27] Spencer, T. J.; Care, C. M.; Amos, R. M.; Jones, J. C. Zenithal bistable device: Comparison of modelling and experiment. *Phys. Rev. E.*, **2010**, *82*, 021702.

[28] Bryan-Brown, G. P.; Walker, D.; Jones, J. C. Method for patterning a surface using selective adhesion. *US patent 0104389 A1,* **2011**.

[29] Jung, G.-Y.; Li, Z.; Wu, W.; Chen, Y.; Olynick, D. L.; Wang, S.-Y.; Tong, W. M.; Williams, R. S. Vapor-phase self-assembled monolayer for improved mold release in nanoimprint lithography. *Langmuir***, 2005**, *21*, 1158-1161.

[30] Xia, Y.; Whitesides, G. M. Soft Lithography. *Ann. Rev. Mat. Sci.*, **1998**, *28*, 153-184.

[31] Amos, R. M.; Bryan-Brown, G. P.; Jones, J. C.; Worthing, P. T. Embossing method and apparatus. *US patent 7824516 B2I,* **2010.**

[32] Blinov, L. M.; Barnik, M. I.; Ohoka, H.; Ozaki, M.; Shtykov, N. M.; Yoshino, K. Surface and flexoelectric polarization in a nematic liquid crystal 5CB. *Eur. Phys. J. E.*, **2001**, *4*, 183-192.

[33] Bogi, A.; Faetti, S. Elastic, dielectric, and optical constants of 4'-pentyl-4-cyanobiphenyl. *Liq. Cryst.*, **2000,** *28*, 729-739.

[34] Basu, R.; Garvey, A.; Kinnamon, D. Effects of graphene on electro-optic response and ion-transport in a nematic liquid crystal. *J. Appl. Phys.*, **2015**, *117*, 074301.

[35] Jones, J. C.; Amos, R. M. Relating display performance and grating structure of a zenithal bistable display. *Mol. Cryst. Liq. Cryst.*, **2011**, *543*, 57-68.

[36] Jung, G.-Y.; Li, Z.; Wu, W.; Chen, Y.; Olynick, D. L.; Wang, S.-Y.; Tong, W. M.; Williams, R. S. Vapor-phase self-assembled monolayer for improved mold release in nanoimprint lithography. *Langmuir*, **2005**, *21*, 1158-1161.

[37] Nguyen, T. P.; Lefrant, S. XPS study of SiO thin films and SiO-metal interfaces. *J. Phys.: Condens. Matter,* **1989**, *1*, 5197-5204.

[38] Wagner, C. D.; Passoja, D. E.; Hillery, H. F.; Kinisky, T. G. Auger and photoelectron line energy relationships in aluminum-oxygen and silicon-oxygen compounds. *J. Vac. Sci. and Tech.*, **1982**, *21*, 933.

[39] Doudevski, I.; Hayes, W.A.; Schwartz, D.K. Submonolayer island nucleation and growth kinetics during self-assembled monolayer formation *Phys. Rev. Lett.,* **1998**, *81 (22),* 4927 – 4930.

[40] Kanta, A.; Sedev, R.; Ralston, J. The formation and stability of self-assembled monolayers of octadecylphosphonic acid on titania. *Colloids and Surfaces A Physicochemical and Engineering Aspects,* **2006**, *91(1-3),* 51 - 58.

[41] McBride, S. P.; Law, B. M. Viscosity-dependent liquid slip at molecularly smooth hydrophobic surfaces. *Phys. Rev. E*, **2009**, *80*, 060601.

[42] Jones, S.A.; Bailey, J; Walker, D.R.E.; Bryan-Brown, G.P.; Jones, J.C. Data for method for tuneable homeotropic anchoring at micro-structures in liquid crystal devices, University of Leeds. [Dataset]. **2018** https://doi.org/10.5518/434

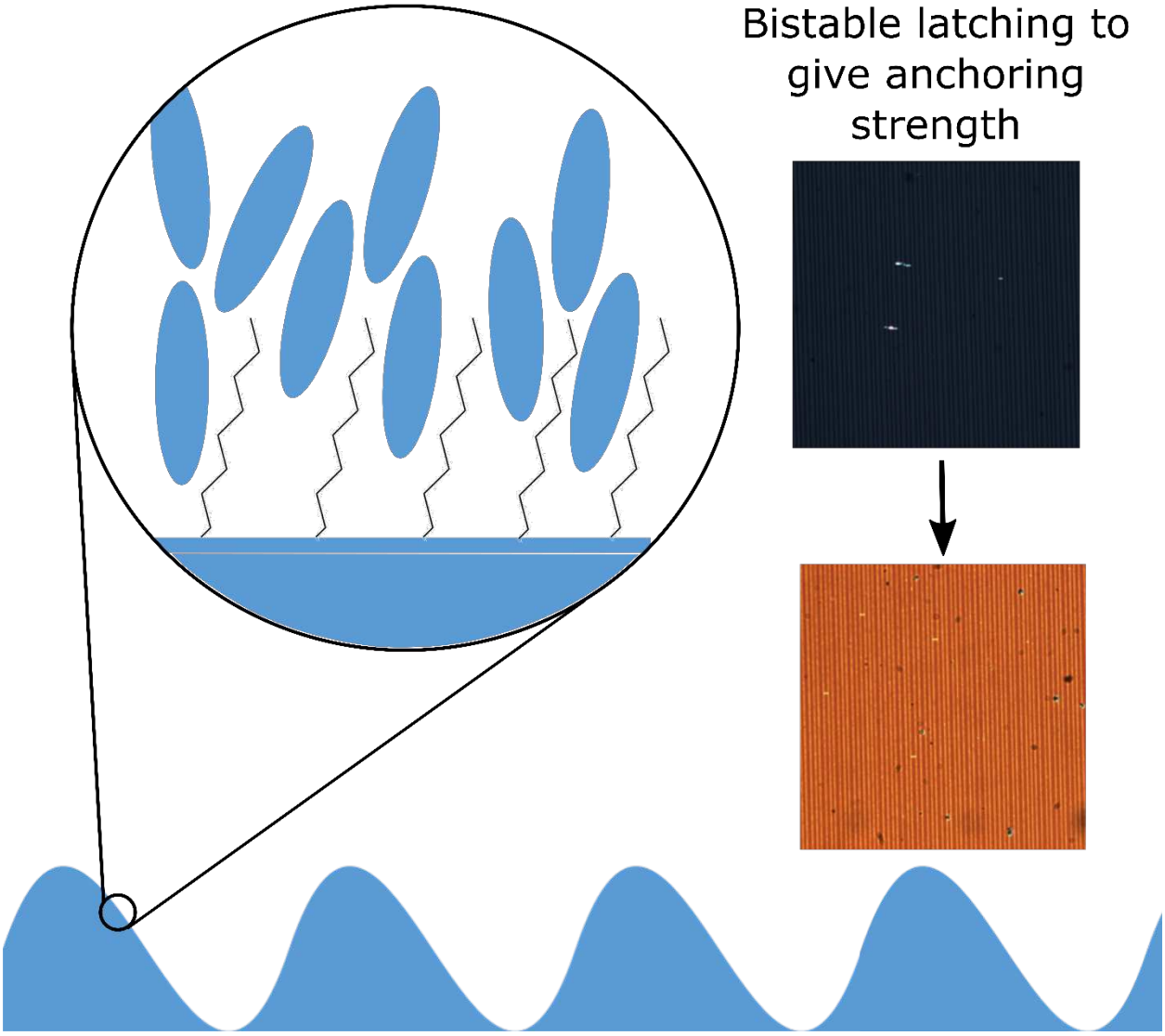

TOC Figure